Available online at www.ilcpa.pl

International Letters of Chemistry, Physics and Astronomy

2 (2015) 100-117 ISSN 2299-3843

Structural and Morphological Studies of Nano-crystalline Ceramic $BaSr_{0.9}Fe_{0.1}TiO_4$

Reenu Jacob[1,a], Harikrishnan G. Nair[2], Jayakumari Isac[2,b]

[1]Department *of Physics,* CMS College, Kottayam, India

[2]Centre for Condensed Matter, Department of Physics, CMS College, Kottayam, India

[a,b]E-mail address: reenujacob12@gmail.com , drjayacmscollege@gmail.com

ABSTRACT

The development of lead-free piezoelectric materials have gained great attention for the consideration of environmental protection. Nanosized $BaSr_{0.9}Fe_{0.1}TiO_4$, a lead free perovskite phase structured ceramic was prepared via a high-energy ball milling process through mechanically assisted synthesis. The sample was analyzed by X-ray Diffraction (XRD), SEM and EDX. The XRD results and XPERT-PRO software analysis confirmed the orthorhombic system of the sample. Scanning Electron Microscopy (SEM) analysis revealed that its crystallite size is in the nano meter range. The grain size was less than 100 nm and showed a strong tendency for agglomeration. It also confirmed with the calculated value from Debye Scherrer's formula. EDX spectrum shows the elemental composition of the sample. Williamson-Hall Plot method was used to evaluate the size and lattice strain. The dislocation density and the morphology index of the sample were also calculated.

***Keywords*:** Barium Strontium Ferric Titanate ($BaSr_{0.9}Fe_{0.1}TiO_4$); Perosvkites; Debye Scherrer formula

1. INTRODUCTION

A characteristic feature of all solid-state reactions is that they involve the formation of product phase(s) at the interfaces of the reactants. The solid-state reactions initiated by intensive milling in high-energy ball mills could be a good choice for the ceramic powder preparation. An important advantage for intensive milling is the formation of highly dispersed phased materials typical for metal powders or oxide based materials (mechanical activation) or the formation of a new product because of a solid-state reaction [1,2]. Intensive milling increases the area of contact between the reactant powder particles due to reduction in crystallite size and allows fresh surfaces to come into contact. As a result, solid-state reactions that normally require high temperatures will occur at lower temperature during mechano chemical synthesis without any externally applied heat. Also, mechanical treatment of ceramic powders can reduce crystallite size and enable obtainment of nano-structured powders, which are of good demand in the current trend of miniaturization and integration of electronic components [3,4]. There has been a continuous succession of new materials and

technology developments leading to a significant number of industrial and commercial applications after the discovery of ferroelectric ceramics in polycrystalline barium titanate.

In the present work the authors describes the preparation of $BaSr_{0.9}Fe_{0.1}TiO_4$ (BSFT) a lead free material since they are now at the top as ferroelectric and piezoelectric materials [5]. This is a nanocrystalline perovskite ceramic material characterized to show good quality, homogeneity and the desired stoichiometry. The results were analyzed by X-ray diffraction (XRD), SEM & EDX. The crystallite size was determined from XRD profile by Debye Scherrer formula. The SEM study reveals that its crystallite size is in nanometer range. The interplanar distance calculated is in confirmation with the theoretical values. The crystallite size and strain of the material is found by Instrumental Broadening and by Williamson-Hall Plot method. The dislocation density and the morphology index of the sample are also calculated.

2. MATERIALS AND METHODS

The perovskite structure is adopted by many oxides that have the chemical formula ABO3. The perovskite like layers can occur as single, double, or triple layers. The representative structure of perovskite compounds is cubic, the compounds in this family may possess some distortion. The orthorhombic and tetragonal phases are the most common variants.

Ceramics with the chemical formula $BaSr_{0.9}Fe_{0.1}TiO_4$ was prepared by the solid state reaction technique according to their molecular formula via a high-energy ball milling process through mechanically assisted synthesis. For preparing sample, the reagent grade chemicals of high purity Barium Carbonate, Strontium Carbonate, Ferric Oxide and Titanium dioxide powders were used as the raw materials and weighed according to their molecular formula,

$$\boldsymbol{BaCO_3 + (SrCO_3)_{0.9} + ½(FeO_3)_{0.1} + TiO_2 \rightarrow BaSr_{.9}Fe_{.1}TiO_4 + 2CO_2.}$$

The required powders were mixed mechanically. Mechanical mixing is usually done by hand mixing in agate mortar for very long time. Then ball milled with zirconium balls to insure homogeneity and milling. The milling conditions are the following: ball-to-powder weight ratio was 40:1 in air atmosphere, basic disc rotation speed was 317/min, rotation speed of disc with jars was 396/min, and the milling time was 32 hrs. After milling the material was calcined at three different temperatures, 30 °C, 550 °C & 850 °C, in a special furnace. The temperature of the furnace is increased in steps. High temperature is needed for metal oxide phase transformations. Control of temperature is often necessary to ensure that the desired crystalline phase is formed and in the optimum particle size [6]. After calcinations, on cooling oxygen flow is allowed into the furnace at fixed intervals (Oxygen Annealing). Further higher temperature resulted the material to harden, difficult to regrind.

2. 1. XRD Analysis

X-ray Diffraction pattern for four different temperatures in steps for the sample $BaSrFeTiO_4$ was taken using Bruker AXS D8 advance diffractometer. The diffractometer with radiations of wavelength 1.54184Å having Nickel filter, equipped with X-ray generator 1140/90/96 having X-ray source KRISTALLOFLXE 780, KF, 4KE with wide angle goniometer PW1710/70 with single pen recorder pm 8203 and channel control PW1390 at 35kV, 10 mA is used for the purpose.

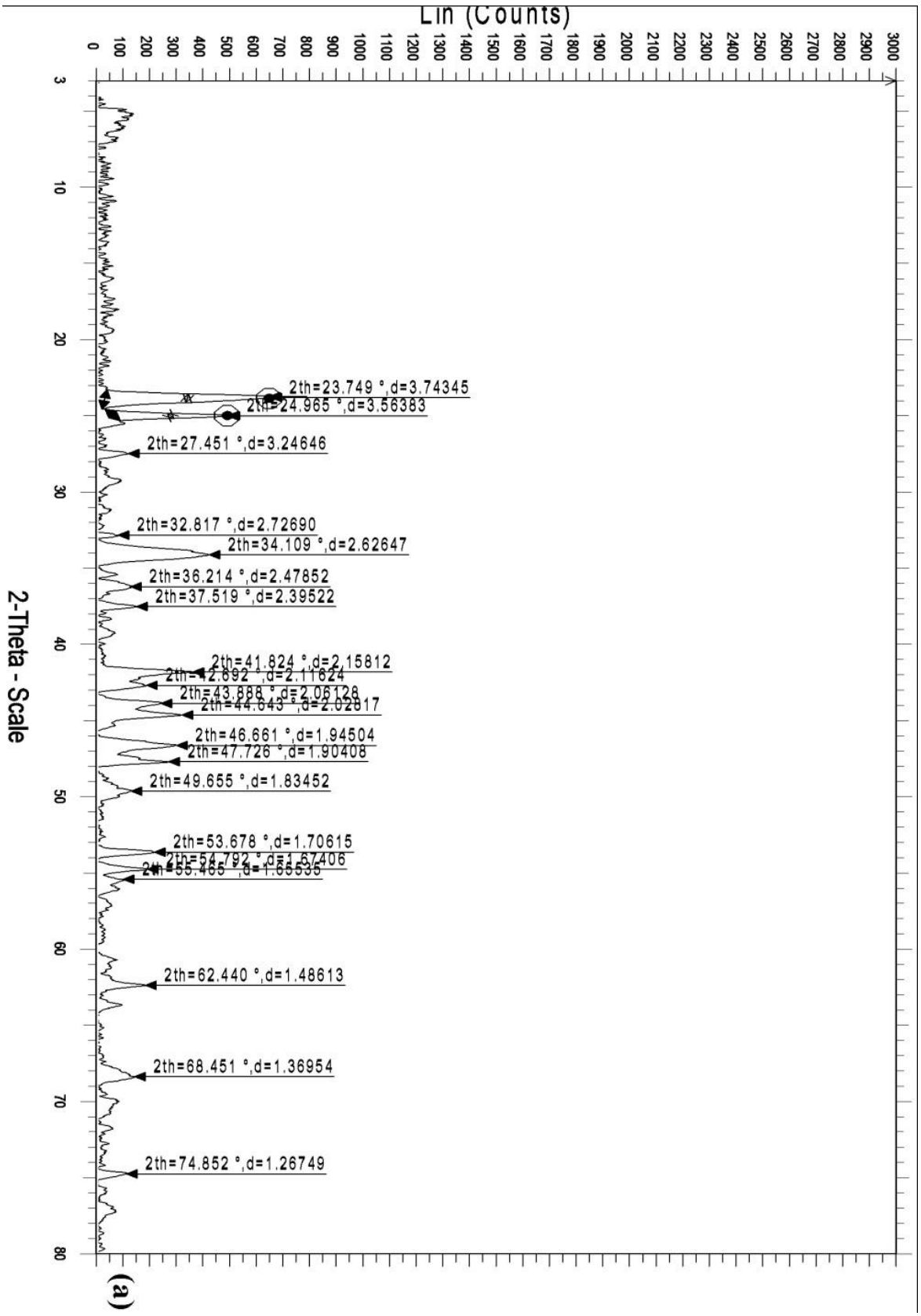
Lin (Counts)
2-Theta - Scale
2th=23.749 °,d=3.74345
2th=24.965 °,d=3.56383
2th=27.451 °,d=3.24646
2th=32.817 °,d=2.72690
2th=34.109 °,d=2.62647
2th=36.214 °,d=2.47852
2th=37.519 °,d=2.39522
2th=41.824 °,d=2.15812
2th=42.892 °,d=2.11624
2th=43.888 °,d=2.06128
2th=44.643 °,d=2.02817
2th=46.661 °,d=1.94504
2th=47.726 °,d=1.90408
2th=49.655 °,d=1.83452
2th=53.678 °,d=1.70615
2th=54.792 °,d=1.67406
2th=55.465 °,d=1.65535
2th=62.440 °,d=1.48613
2th=68.451 °,d=1.36954
2th=74.852 °,d=1.26749
(a)

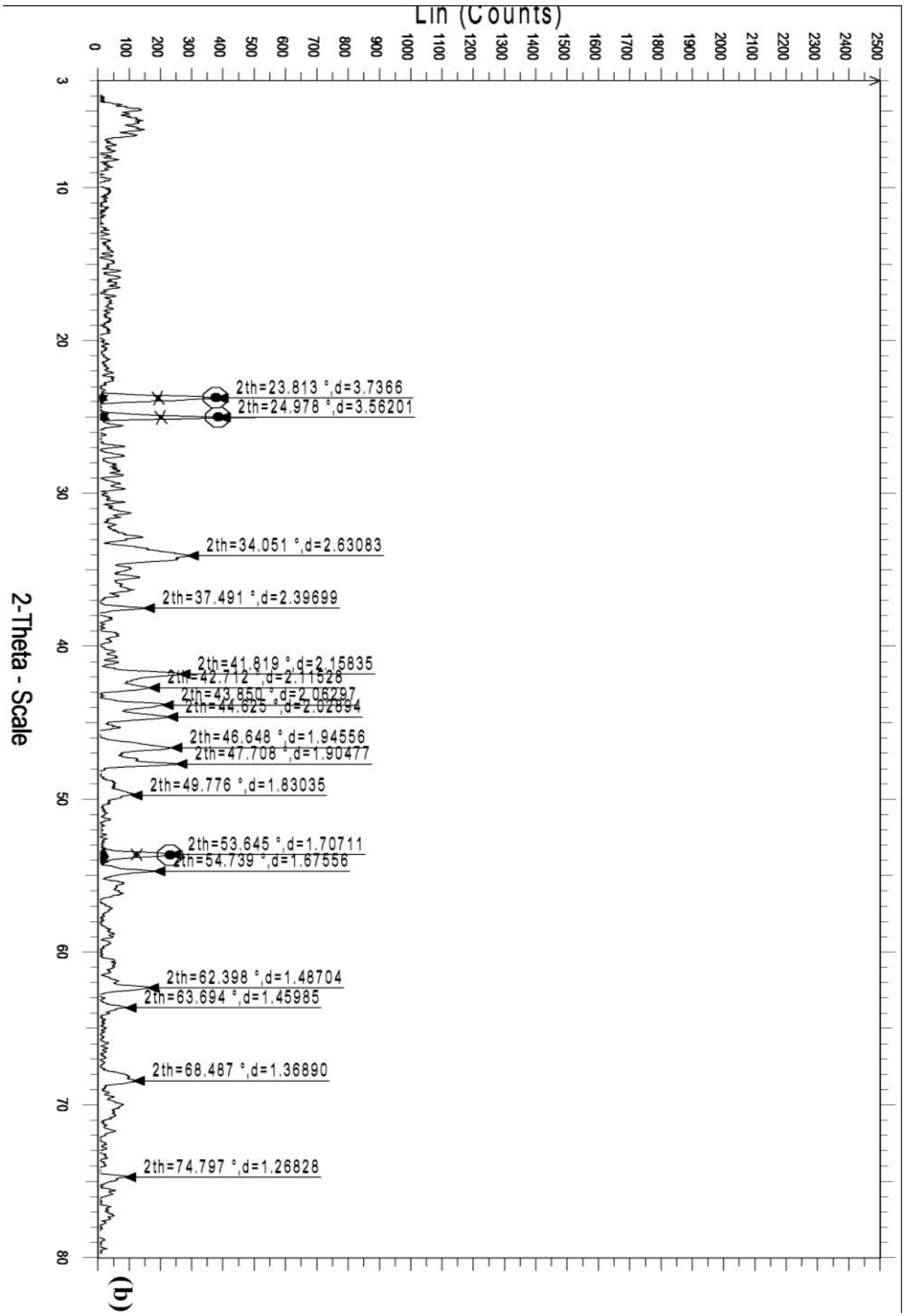
Lin (Counts)
0
100
200
300
400
500
600
700
800
900
1000
1100
1200
1300
1400
1500
1600
1700
1800
1900
2000
2100
2200
2300
2400
2500
2-Theta - Scale
3
10
20
30
40
50
60
70
80
2th=23.813 °,d=3.7366
2th=24.978 °,d=3.56201
2th=34.051 °,d=2.63083
2th=37.491 °,d=2.39699
2th=41.819 °,d=2.15835
2th=42.712 °,d=2.11528
2th=43.850 °,d=2.06297
2th=44.625 °,d=2.02894
2th=46.648 °,d=1.94556
2th=47.708 °,d=1.90477
2th=49.776 °,d=1.83035
2th=53.645 °,d=1.70711
2th=54.739 °,d=1.67556
2th=62.398 °,d=1.48704
2th=63.694 °,d=1.45985
2th=68.487 °,d=1.36890
2th=74.797 °,d=1.26828
(b)

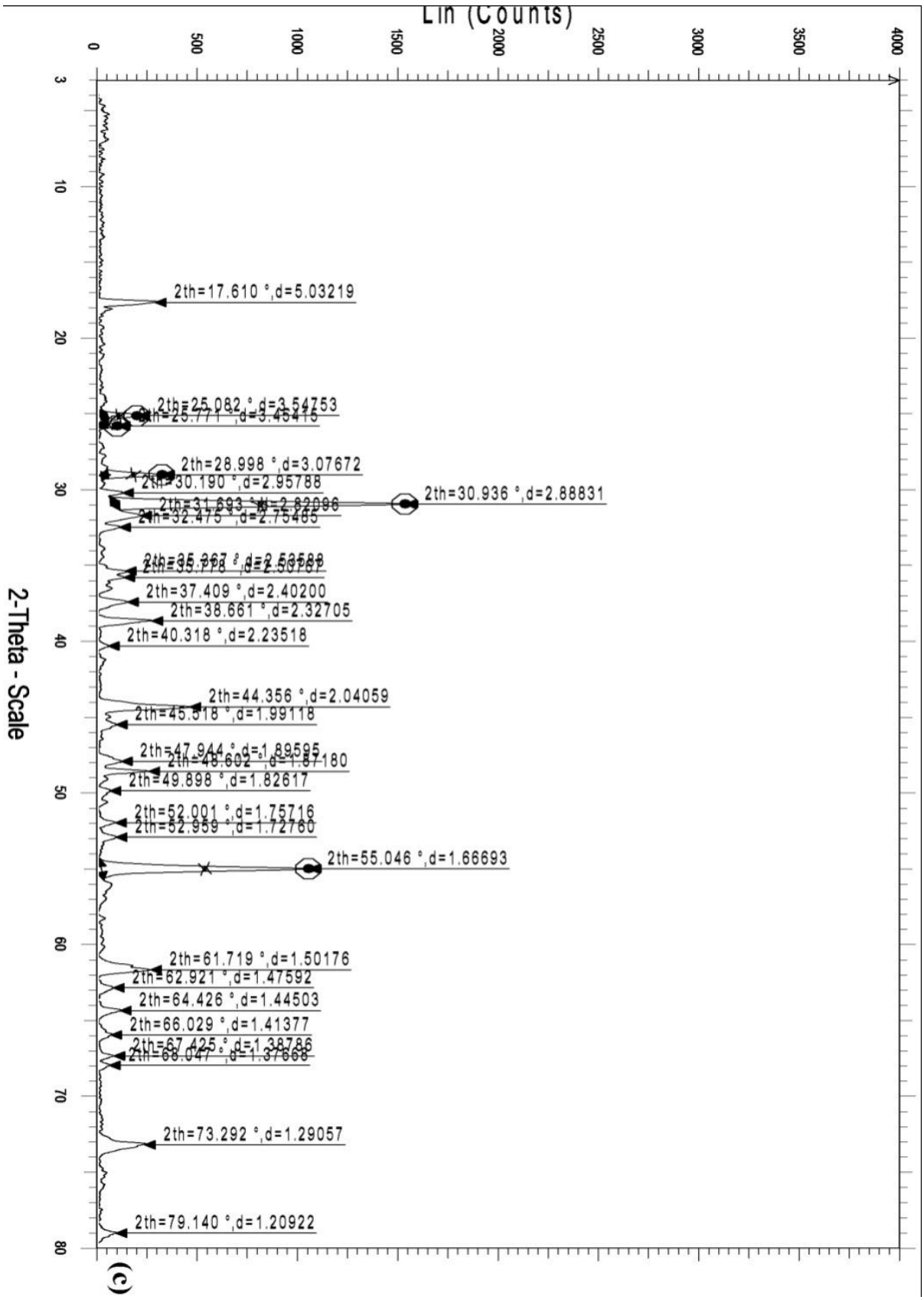

Figure 1. XRD pattern of $BaSr_{0.9}Fe_{0.1}TiO_4$ - at three temperatures (a) 30 °C, (b) 550 °C & (c) 850 °C .

The scanning speed of the specimen is 2 degree/minute. From the XRD results and XPERT-PRO software analysis, the crystal BSFT was found to be orthorhombic system with $a \neq b \neq c$ **and** $\alpha = \beta = \gamma = 90^{\circ}$. a =11.0587Å , b = 7.1639Å , c = 4.6569Å, $\alpha = \beta = \gamma = 90^{\circ}$.

2. 2. Crystallite Size Measurements

Crystal structure was solved by analyzing the intensities of diffracted X-ray beams and by using the XPERT-PRO software analysis. X-ray diffraction profile is used to measure the average crystallite size of the sample provided the average diameter was less than 200 Å. The lines in a powder diffraction pattern are of finite breadth but since the particles were very small, the lines started to broaden than usual.

The broadening decreases with the increase in crystallite size. The crystallite size for $BaSr_{0.9}Fe_{0.1}TiO_4$ was calculated from X-ray diffraction profiles of strong reflections with intensity % by measuring the full width at half maximum (FWHM).

The Debye Scherrer equation for calculating the crystallite size is given by

$$D = \frac{K\lambda}{\beta cos\theta} (1)$$

where K is the Scherrer constant, λ is the wavelength of light used for the diffraction, β the "full width at half maximum" of the sharp peaks, and θ the angle measured. The Scherrer constant (K) in the above formula accounts for the shape of the particle and is generally taken to have the value 0.9. The results revealed that the crystallite size is less than 100 nm.

2. 3. Calculation of d-Spacing

The value of d (the inter planar spacing between the atoms) is calculated using the **Bragg's Law**, $2d\,sin\,\theta = n\lambda$ or $d = \frac{\lambda}{2\,sin\,\theta n(n=1)}$ (2) Wavelength of X ray = 1.5 Å for CuKα.

Table 1. Crystallite size of $BaSr_{0.9}Fe_{0.1}TiO_4$ at different temperatures and the inter planar spacings calculated are listed below.

Data of high intensity peak of XRD at different temperatures	2θ (°)	FWHM(β) (rad.)	Crystallite size (nm)	d in A° (observed)	d in A° (calculated)
$BaSr_{.9}Fe_{.1}TiO_4$ at 30 °C	23.749 24.965	0.01022 0.00749	13.8747 18.9752	3.722 3.566	3.745 3.565
$BaSr_{.9}Fe_{.1}TiO_4$ at 550 °C	23.813 24.978	0.00666 0.00612	21.2937 23.2230	3.711 3.55	3.734 3.563
$BaSr_{.9}Fe_{.1}TiO_4$ at 850 °C	25.082 25.771	0.00452 0.00405	31.4507 35.1568	3.549 3.455	3.549 3.455

Table 2. The (hkl) indices calculated from the 2 θ values of the XRD profile are listed below.

2 θ in degrees	*hkl*
25.082	211
28.998	400
30.936	410
35.267	321
40.318	222
44.356	402
45.518	431
47.944	003
55.046	323

2. 4. XRD-Instrumental Broadening

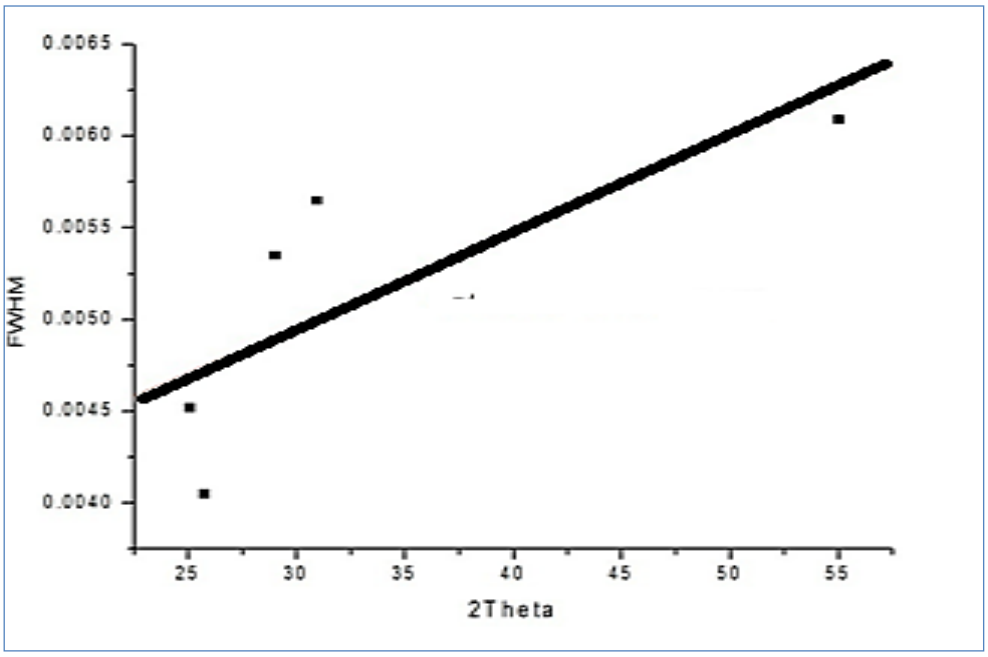

Figure 2. Typical Instrumental Broadening.

When crystallite size is less than 100 nm, appreciable broadening in X-ray diffraction lines will occur. Diffraction pattern will show broadening because of reduction in the crystallite size and strain. The observed line broadening will be used to estimate the average size of the particles. The total broadening of the diffraction peak is due to sample and the instrument.

The sample broadening is described by

$$\boldsymbol{FW(s) \times cos\,\theta = \frac{K\lambda}{size} + 4strain \times sin\,\theta} \quad (3)$$

The total broadening, β_t equation is described from Sample broadening and instrumental broadening as

$$\boldsymbol{\beta_t^2 \approx \left\{\frac{0.9\lambda}{Dcos\theta}\right\}^2 + \{4\varepsilon tan\theta\}^2 + \beta_0^2} \quad (4)$$

where D is average crystallite size, ε is strain and βo is instrumental broadening. Instrumental broadening is presented in the Figure 2.

2. 5. Williamson-Hall Plot

This method is attributed to G. K. Williamson and his student, W. H. Hall. It relies on the principle that the approximate formulae for size broadening, and strain broadening, vary quite differently with respect to Bragg angle, θ. Williamson and Hall proposed a method for deconvoluting size and strain broadening by looking at the peak width as a function of 2θ.

$$\boldsymbol{FW(s) \times cos\,\theta = \frac{K\lambda}{size} + 4strain \times sin\,\theta} \quad (3)$$

One contribution varies as 1/cosθ and the other as tan θ. If both contributions are present then their combined effect should be determined by convolution. The simplification of Williamson and Hall is to assume the convolution is either a simple sum / sum of squares. Comparing this to the standard equation for a straight line, y = mx + c. We see that by plotting FW(s) cos θ versus sin θ we obtain the strain component from the slope and the size component from the y- intercept. Such a plot is known as a Williamson-Hall Plot.

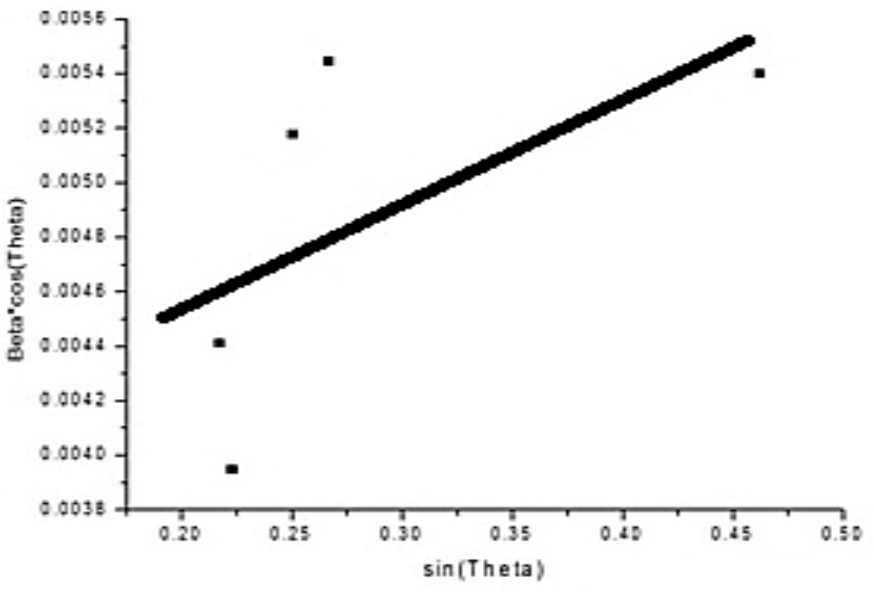

Figure 3. Williamson Hall Plot.

Table 3. Crystallite size of the sample at 850^0C measured from different methods.

1. Using Debye Scherrer formula, crystallite size = 31.4507 nm, 35.1568 nm.
2. Using Williamson Hall Plot, crystallite size = 30.689 nm.

2. 6. XRD-Dislocation Density(δ)

The dislocation density is defined as the length of dislocation lines per unit volume of the crystal [10]. Chen and Hendrickson measured and determined dislocation density and hardness of several crystals. Theoretically a dislocation is a crystallographic irregularity or a defect formed within the crystal. The properties of the crystal formed are strongly influenced by the defects inside the crystal. Shift or movement of a dislocation is impeded by other dislocations present in the sample. They found that crystals with larger dislocation density were harder [11]. It has been shown that the dislocation density increases while grain size decreases with increasing strain and ultimately these parameters reach saturation values [12]. Above a certain crystallite size limit (~20 nm) the strength of materials increases with decreasing crystallite size [13]. The dislocation density (δ) in the sample has been determined using values of FWHM, θ, lattice constant and particle size [14]. The number of unit cell is calculated from crystallite size and cell volume of the sample [15].

$$(\delta) = 15\beta\cos\theta/4aD,$$

where **β** the FWHM measured in radians**, θ** the diffracting angle, **a** the cell parameter and **D** is the crystallite size in nm, depicted in Table 4.

Table 4. The variation of **(δ)** with the crystallite size is given below.

Data of high intensity peak of XRD at different temperatures	**2θ (°)**	**FWHM(β) (rad)**	**Crystallite size (nm)**	(δ) $X10^{15}$	No of unit cells $X10^4$
$BaSr._9Fe._1TiO_4$ at 30 °C	23.749 24.965	0.01022 0.00749	13.8747 18.9752	2.445 1.3064	0.3621 0.9242
$BaSr._9Fe._1TiO_4$ at 550 °C	23.813 24.978	0.00666 0.00612	21.2937 23.2230	0.9615 0.8725	1.3089 1.6983
$BaSr._9Fe._1TiO_4$ at 850 °C	25.082 25.771	0.00452 .004049	31.4507 35.1568	0.4759 0.3807	4.2181 5.8918

The crystallite size D can be measured from the Debye Scherrer formula as

$$\mathbf{D = 0.9\lambda /\beta \cos\theta} .$$

The no. of unit cells**,**

$$\mathbf{n = \pi\ x(4/3)(D/2)^3\ x1/V},$$

where **V** is the cell volume of the sample. V = 368.9355Å.

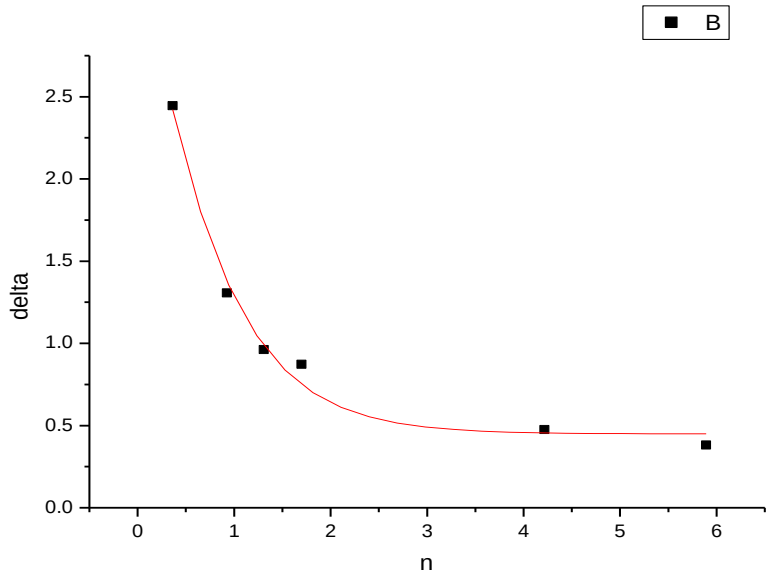

Fig. 4.1. n vs. Dislocation Density (δ),

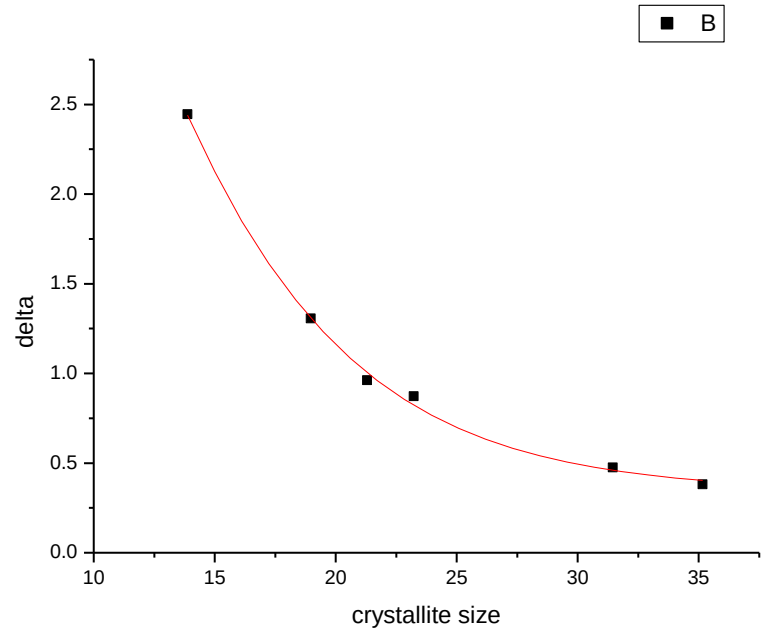

Fig. 4.2. crystallite vs. delta, n.

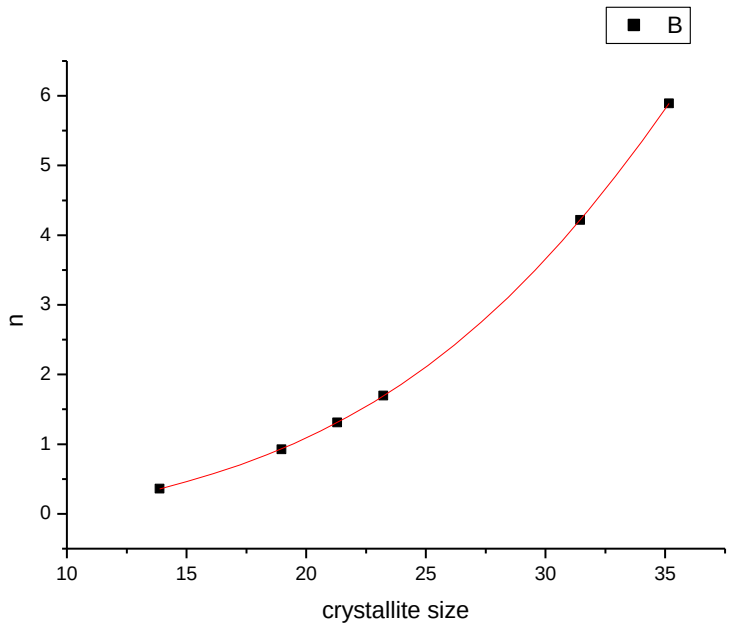

Fig. 4.3. crystallite vs. delta, n.

From the plots (Fig. 4.1-4.3) it is confirmed that dislocation density is indirectly proportional to particle size and number of unit cell. Dislocation density decreases when both particle size and number of unit cell increases.

2. 7. XRD-- Morphology Index

Sharper XRD peaks are typically indicative of high nano crystalline nature and larger crystallite materials. From the XRD data, a peak broadening of the nano particles is noticed. Morphology Index (MI) is calculated from FWHM of XRD data. It is observed that MI has direct relationship with crystallite size and an inverse relationship with specific surface area.

The Morphology – Index is calculated as,

$$\mathbf{MI = FWHMh/(FWHM_h + FWHM_p)} ,$$

where $\mathbf{FWHM}_h$ represents the highest FWHM value of the diffracted peak at a particular value of **D** (crystallite size in nm) and $\mathbf{FWHM}_p$ stands for the value of the particular peak for which the **MI** has to be calculated. The calculated values of the **MI** are listed below. The graph showing the relation of MI with D is shown in Fig. 5.

Table 5. The relation between MI and D.

β in radians	D in nm	MI
.00749	18.9752	0.513
.00612	23.2230	0.577
.004049	35.1568	0.623

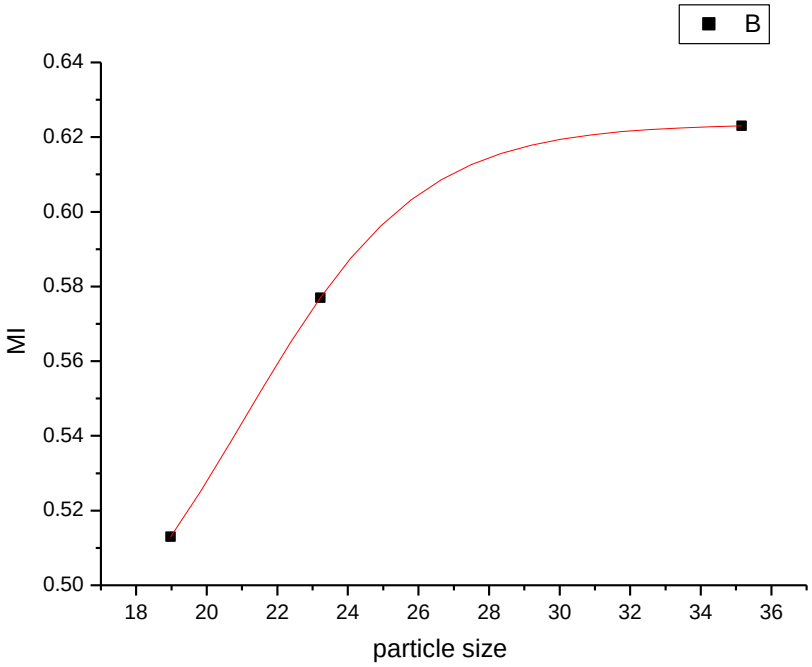

Fig. 5. The relation of MI with D.

Table 5. The relation between MI and D.

β in radians	D in nm	MI
.00749	18.9752	0.513
.00612	23.2230	0.577
.004049	35.1568	0.623

From the graph (Fig. 5) shown it is very clear that MI of a particular sample is directly related to its crystallite size.

2. 8. SEM Analysis - Morphology studies

The SEM analyses gives the surface of solid objects, producing images of higher resolution than optical microscopy and produces representations of the sample under study. Figure 6 shows the surface morphology of $BaSr_{0.9}Fe_{0.1}TiO_4$.

The crystallite size measurement through SEM revealed that its maximum dimension is always less than 100 nm.

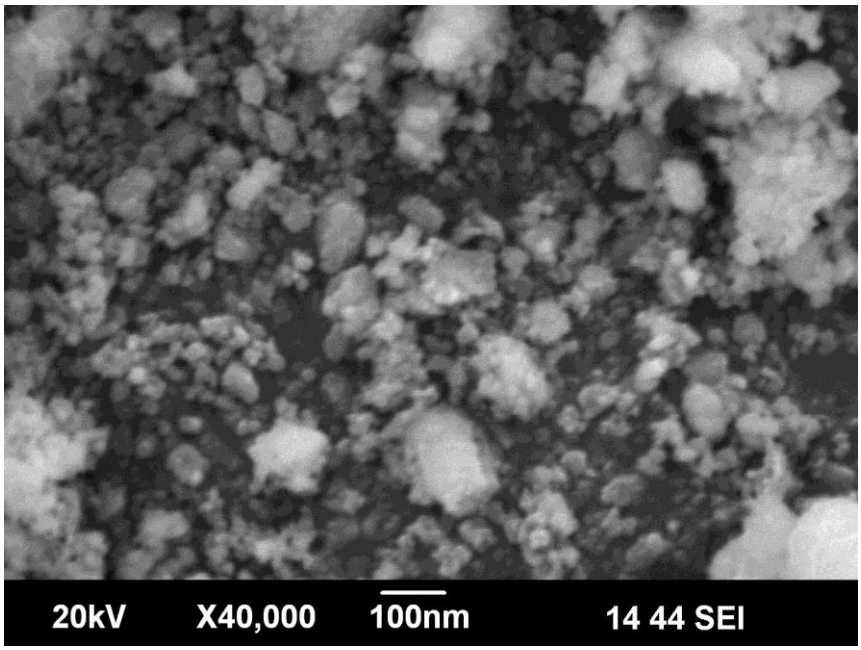

(a)

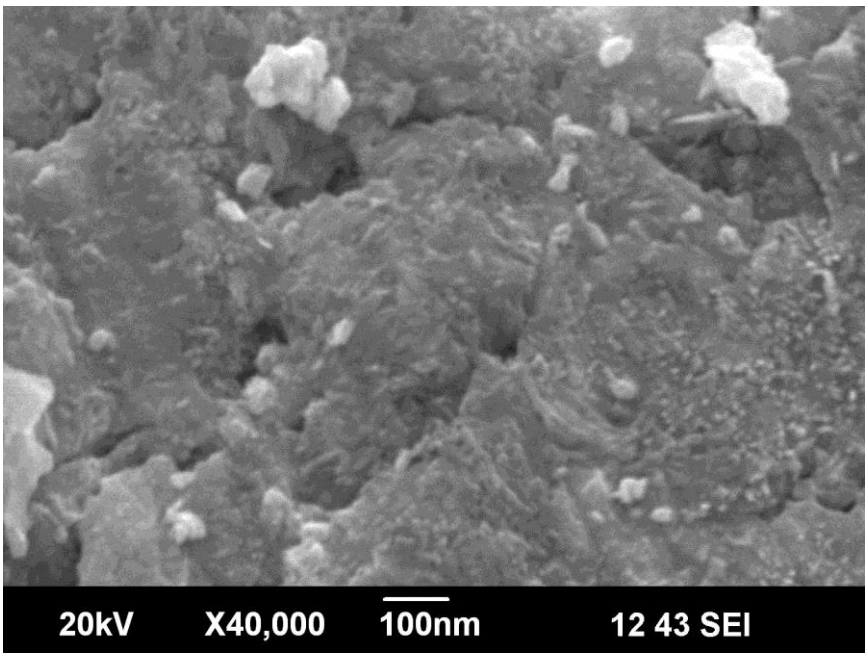

(b)

Figure 6. SEM photograph of $BaSr_{.9}Fe_{.1}TiO_4$ (a) 550 °C, (b) 850 °C

The SEM analyses gives the surface of solid objects, producing images of higher resolution than optical microscopy and produces representations of the sample under study. Figure 6 shows the surface morphology of $BaSr_{0.9}Fe_{0.1}TiO_4$. The crystallite size measurement through SEM revealed that its maximum dimension is always less than 100 nm.

2. 9. Energy Dispersed X-Ray Spectrograph (EDX)

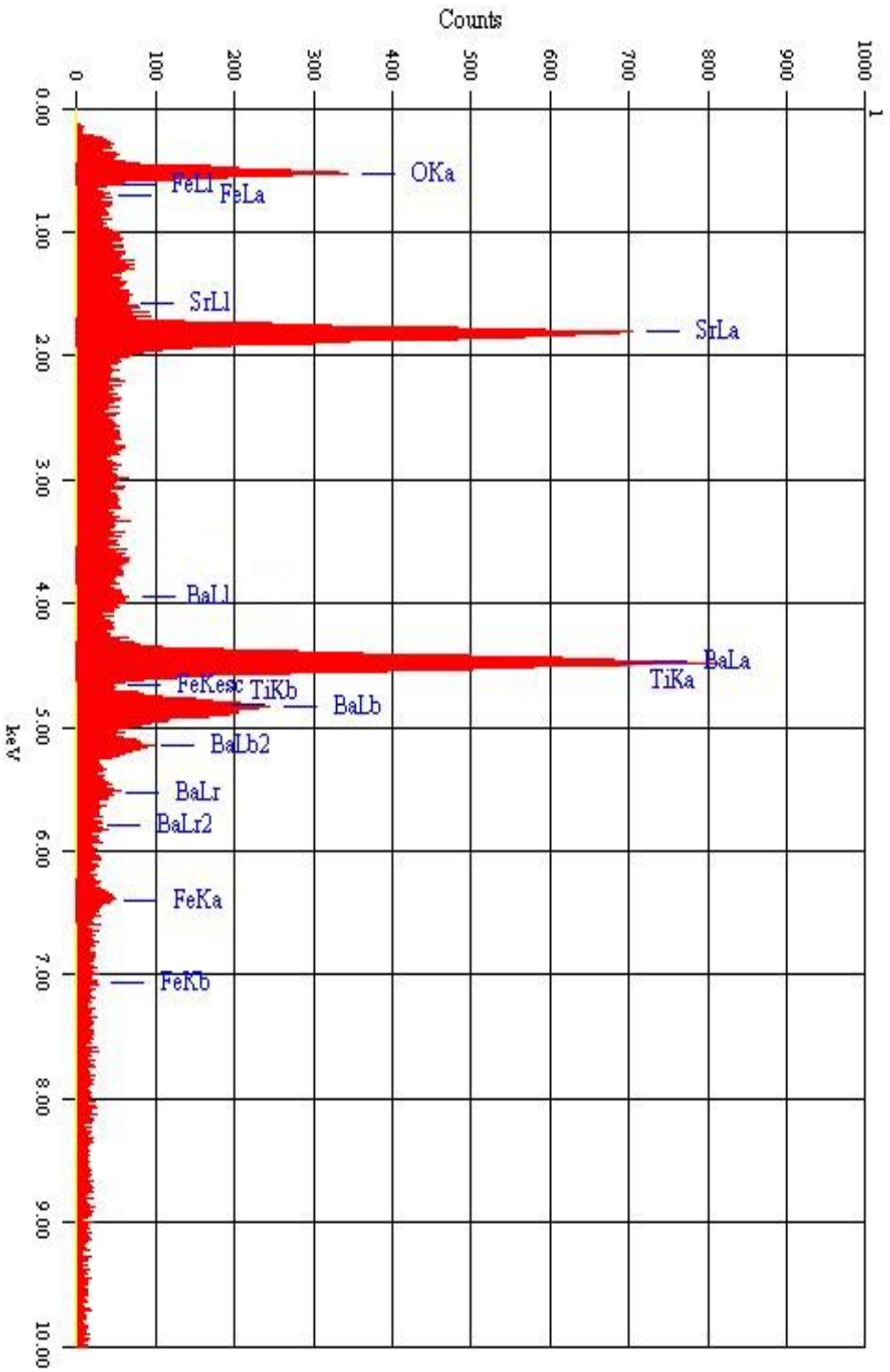

Figure 7. EDX of $BaSr_{0.9}Fe_{0.1}TiO_4$

EDX shows the composition details of the prepared ceramic powders (Figure 7). The instrument used for this measurement is ISIS Link Oxford Instrument UK. This technique is generally associated with Scanning Electron Microscope (SEM). In this technique an electron beam of 10-20 KeV strikes the surface of a sample which causes X-ray to be emitted from point of incidence.

The energy of the X-ray emitted depends on material under examination. When an X-ray strikes the detector, it will generate a photoelectron which in turn generates electron-hole pairs. A strong electric field attracts the electrons and holes towards the opposite ends of the detector. The size of the pulse thus generated depends on the number electron hole pairs created, which in turn depends on the energy of the incoming X-ray. In this method however elements with low atomic number are difficult to be detected.

The detector which is lithium doped silicon is protected by a beryllium window and operated at liquid nitrogen temperatures. The absorption of the soft X-rays by the beryllium decreases the sensitivity below an atomic number 11.

The EDX spectrum (Fig. 7) obtained give the composition of the material under study.

Table 6. Material Content from (EDX).

Material	content(%)
Ba	44
Sr	27
Fe	2.14
Ti	2.01
O	24.85

From the EDX spectrum, the four dominant peak positions at 4.465keV (Ba Lα), 5.1,.5,5.8keV (Ba Lβ, Lγ, Lγ2), 1.806keV (Sr Lα), 0.705, 6.398keV (Fe Lα, Kα), 0.452, 4.508keV (Ti Lα, Kα), 0.525keV (O Kα) correspond quite well to the energy pattern of the corresponding materials (Ba, Sr, Fe, Ti, and O) reported in the EDAX international chart. Table 6, shows the percentage of the elements in the prepared $BaSr._9Fe._1TiO_4$ sample.

3. RESULTS & DISCUSSIONS

The XRD patterns of BaSrFeTiO4 powder obtained for various annealing temperatures are shown in Figure 1. XRD spectrum for the different temperatures gave a clear idea about the maximum intensity peak shifting corresponds to the different treating temperatures. As the temperature increases, the highest peaks in the XRD spectrums shifts from left to right through the 2θ axis and the highest intensity peak decreases.

The atoms undergo thermal vibration about their mean positions even at the absolute zero of temperature, and the amplitude of this vibration increases as the temperature increases. Increased thermal vibration of the atoms, as the result of an increase in temperature, the unit cell expands, causing changes in d spacing and therefore in the 2θ positions of the diffraction lines. And also the intensities of the diffraction lines decrease. When the material is cooled to room temperature, the amplitude of the atomic vibrations of the material was decreased.

But it couldn't arrive at the initial amplitude. The atomic vibration amplitude of the heated material was higher than initial amplitude.

As the atomic vibration amplitude increases, the intensity of the diffracted beam also decreases because it has the effect of smearing out lattice planes. Thus the reinforcement of waves scattered at the Bragg angle by various parallel planes is not as perfect as it is for a crystal with fixed atoms.

This reinforcement requires that the path difference, which is a function of the plane spacing d, between waves scattered by adjacent planes should be an integral number of wavelengths. From Figure 1, the peak broadening in the XRD patterns clearly indicated the nature of formation of the very small nano crystals. From the width of the XRD peak, the mean crystallite size is calculated using Debye Scherrer's equation. From Table 1, it is confirmed that crystallite size of the material $BaSr._9Fe._1TiO_4$ increases with respect to the treating temperature increase.

The results revealed that the crystallite size is less than 100 nm. The diffraction data revealed that the material belongs to orthorhombic system.. Heat treatment causes the particles to anneal and form larger grains, which of course indicates that the particles become larger. Hence, the large size of sample at 850 °C is expected. This also agrees with the high crystallinity, as having larger grains means more long-range order, and hence more crystallinity [7,8].

The value of inter planar distance for different values of θ are calculated and tabulated which is found to be in good agreement with the observed results. It is tabulated in Table 1. The hkl values calculated from the XRD profile are listed in the Table 2.

The dislocation density (δ) is determined from the XRD profile. It is clearly confirmed that dislocation density decreases as the crystalline sized increases. Higher value of dislocation density results in greater hardness. The no. of unit cells also is found to have an inverse relation with the dislocation density. Morphology Index (MI) is calculated and observed that MI has direct relationship with crystallite size.

Figure 8 shows SEM image of $BaSr_{0.9}Fe_{0.1}TiO_4$. The SEM photograph revealed maximum dimensions of the particles to be always less than 100 nm. This is an experimental proof of the theoretical calculation of particle size by Debye Scherrer equation from XRD data. EDX spectrum (Fig.7) gives the information on the elemental composition of $BaSr_{0.9}Fe_{0.1}TiO_4$. The elemental compositions agree with the chemical formula of the prepared compound. The EDX spectrum obtained give the confirmation of the elemental composition of the material under investigation. The size and strain of the experimentally observed broadening of several peaks (Fig. 2) are computed simultaneously using least squares method. The broadening of peak may also occur due to micro strains of the crystal structure arising from defects like dislocation and twinning [9]. Here, Williamson-Hall plot is plotted with sinθ on the x-axis and βcosθ on the y-axis (in radians). The extracted particle size is 30.689nm and strain is .0091257 from Williamson Hall Plot.

4. CONCLUSIONS

In this work the lead free ceramic $BaSr._9Fe._1TiO_4$ was prepared successfully by the conventional solid state reaction technique and analysed by XRD, SEM& EDX. XRD data confirmed the formation of the perovskite phase structure and the average crystallite size. The XRD spectrums of the $BaSr._9Fe._1TiO_4$ at different temperatures indicate that, according to increasing treating temperature, the θ value and crystallite size also increases.

As the temperature is increased the band gap decreases and hence peaks get broadens. From SEM analysis, the morphology images show the approximate size of the nano particles. The value of crystallite size calculated from the Williamson-Hall plot method is in agreement with that of the crystallite size measured from Debye Scherrer formula.

The dislocation density (δ) is determined and confirmed that dislocation density decreases as the crystalline size increases. Higher value of dislocation density results in greater hardness. The no. of unit cells also is found to have an inverse relation with the dislocation density. Morphology Index (MI) is calculated and observed that MI has direct relationship with crystallite size. The EDX analysis indicates that the elements exist in the sample and they agree with the chemical formula of the prepared compound. The mechano chemical process has an advantage due to low-costs and widely available materials, leading to a simplified process.

Acknowledgement

The authors are thankful to SAIF, Kochi for providing the data analysis and to the Principal, CMS College, Kottayam, Kerala for providing the facilities.

References

[1] J. Wang, D. Wan, J. M. Xue, W. B. Ng, Singapore Patent 9801566-2, 1998.
[2] J. Xue, D. Wan, S. E. Lee, J. Wang, *J. Am. Ceram. Soc.* 82 (1999) 1687.

[3] J. Ding, T. Suzuki, P. G. McCormic, *J. Am. Ceram. Soc.* 79 (1996) 2956.

[4] A. K. Giri, *Adv. Mater.* 9 (1997) 163.

[5] Rigoberto López-Juárez, Federico González and María-Elena Villafuerte-Castrejón DOI: 10.5772/20107. Lead-Free Ferroelectric Ceramics with Perovskite Structure.

[6] Ceramic materials-science and engineering, www.golsarfars.com/userfiles/file/part-3.pdf

[7] Xie, Q. and McCourt, F. (2008) Nanotechnology Engineering NE 320L Lab Manual. University of Waterloo, Waterloo, 35-39.

[8] So W.W., Jang J.S., Rhee Y.W., Kim K.J., Moon S.J., *Journal of Colloid and Interface Science* 237 (2001) 136-141.

[9] Ghosh, S.C. and Thanachayanont, C. and Dutta, J. (2004) Studies on Zinc Sulphide Nanoparticles for Field Emission Devices. The 1st ECTI Annual Conference (ECTI-CON2004), Pattaya, McCourt, F. (2008) Nanotechnology Engineering NE 320L Lab Manual. University of Waterloo, Waterloo, 35-39.

[10] Thirugnanasambandan Theivasanthi, Marimuthu Alagar -- Konjac Biomolecules Assisted–Rod/ Spherical Shaped Lead Nano Powder Synthesized by Electrolytic Process and Its Characterization Studies -Nano Biomed Eng, Article, ISSN 2150-5578 http://nanobe.org

[11] Sirdeshmukh D.B., Sirdeshmukh L., Subhadra K.G. Micro- and macro-properties of solids: thermal, mechanical and dielectric properties. Springer, NewYork. 2006.

[12] Chinh N.Q., Gubicza J., Langdon T.G., *J. Mater. Sci.* 5 (2007) 1594-1605.

[13] Weertman J.R., *Mater. Sci. Eng. A.* 166(1-2) (1993) 161-167.

[14] Subbaiah Y.P.V., Prathap P., Reddy K.T.R., *Appl. Surf. Sci.* 253(5) (2006) 2409-2415.

[15] Sing P., Kumar A., Kaushal A., Kaur D., Pandey A., Goyal N., *Bull. Mater. Sci.* 31(3) (2008) 573-577.

(Received 22 October 2014; accepted 01 November 2014)